Engineering Structures 65 (2014) 89–98

Contents lists available at ScienceDirect

Engineering Structures

journal homepage: www.elsevier.com/locate/engstruct

Optimal placement of nonlinear hysteretic dampers on planar structures under seismic excitation

Carlos A. Martínez, Oscar Curadelli *, María E. Compagnoni

Engineering Faculty, National University of Cuyo, CONICET, Mendoza, Argentina

ARTICLE INFO

Article history:
Received 26 June 2013
Revised 11 November 2013
Accepted 20 January 2014

Keywords:
Optimal hysteretic dampers placement
Equivalent linearization
Stochastic analysis

ABSTRACT

In the last twenty years great efforts were carried out to develop the concept of energy dissipation in structures to bring it into an applicable technology. Several devices based on different energy dissipation principles have been developed and implemented worldwide. One of the most important tasks for the designer is to define the locations and sizes of these devices in order to maximize their efficiency and safety. In this work, an efficiently procedure to optimally define the energy dissipation capacity of added nonlinear hysteretic dampers, to meet an expected level of performance on planar structures under seismic excitation is proposed. Knowing that the main contribution to the total uncertainty is due to the excitation and with the aim of achieving a robust design, the excitation is modeled as a stationary stochastic process characterized by a power spectral density compatible with a response spectrum defined by seismic code provisions of the region. Since the analysis is performed in the frequency domain, the nonlinear behavior of dampers is included through stochastic equivalent linearization of Bouc–Wen hysteretic model. The proposed procedure is verified numerically through nonlinear time history analysis using artificial ground motion records.

1. Introduction

It is well known that, in order to reduce the structural response, external energy dissipation devices may be advantageously used. The effectiveness of these systems depends on the type and capacity of energy dissipation, as well as, the placement of dampers into the structure. In view of these considerations, optimum design studies on energy dissipation systems have been of great interest, principally in earthquake engineering over the last twenty years.

Optimal placement of linear devices (viscous and viscoelastic) have been extensively discussed in the scientific literature. Many research papers have been published in the last two decades [1–12] in which most of the optimization methods were based on transfer functions of structural parameters such as the sum of interstory drift, top displacement, top absolute acceleration and base shear. Other important strategies that make use of genetic algorithms were developed by Singh and Moreschi [13] and Bishop and Striz [14]. A gradient-based method including a performance index defined as a weighted combination of displacements, drifts and absolute accelerations was presented by Singh and Moreschi [15].

With regard to the optimization of nonlinear dissipation systems, Uetani et al. [16] described an optimum structural design method for building frames provided with hysteretic dampers. Ni et al. [17] estimated the stochastic seismic response of adjacent structures connected with hysteretic nonlinear dampers, using the statistical linearization technique and considering that the structure remains in elastic range. Through a parametric study, the authors showed the existence of optimum parameters in metallic dissipation systems. Basili and De Angelis [18] explored the same idea of interconnected structures with hysteretic devices under filtered white noise excitation using a stochastic equivalent linearization technique. The efficiency of the control system was assessed through a performance index which takes into account the ratio between the energy dissipated in the devices and the seismic energy entering into the structure. A similar study, but using genetic algorithm was published by Ok et al. [19]. Moreschi and Singh [20] presented a methodology conducted in time domain, also based on genetic algorithms, to define optimal design parameters in dissipation systems that use yielding metallic and friction dampers. Jensen [21] investigated the optimization of nonlinear systems through the statistical equivalent linearization technique, using as objective function a linear combination of the statistical

* Corresponding author. Address: Facultad de Ingeniería, Centro Universitario, Parque Gral. San Martín, 5500 Mendoza, Argentina. Tel.: +54 261 4135000 2195; fax: +54 261 4380120.
E-mail address: ocuradelli@fing.uncu.edu.ar (O. Curadelli).

http://dx.doi.org/10.1016/j.engstruct.2014.01.030
0141-0296/

moments of the structural response. Vargas and Bruneau [22] studied the effectiveness on the reduction of lateral displacement and acceleration of one degree of freedom systems, in which viscous and metallic dampers work together. Based on the results of a parametric study on nonlinear SDOF systems subjected to synthetic ground motions, Vargas and Bruneau [23] proposed a structural fuse design procedure for MDOF structures. The study was carried out using buckling-restrained braces used as metallic structural fuses and verified by experimental tests performed on a shaking table at the University at Buffalo. Jensen et al. [24] presented a methodology based on reliability, for optimizing structural systems under stochastic excitation, using a linear search algorithm. Later, Jensen and Sepúlveda [25] proposed a similar procedure to design structures equipped with dissipation systems, taking into account the uncertainties of the structure and excitation. Benavent-Climent [26] developed a method to determine lateral strength, stiffness and energy dissipation capacity of the hysteretic devices needed in each story to achieve a prescribed target performance for a given seismic hazard. Leu and Chang [27] proposed a relocation strategy of nonlinear viscous dampers in 3D structures. The procedure starts from a uniform distribution and then iteratively moves the dampers to positions of maximum interstory drift. Ohsaki and Nakajima [28] presented an optimization method to design eccentrically braced frames, in which the plastic deformation in the link is used as energy dissipating device.

While many studies have been proposed to optimize viscous damper placement, only a few of them deal with nonlinear dampers and explicitly define the total capacity of the dissipation system to achieve an expected seismic performance. In this paper, a simple procedure to optimally define the location and size of nonlinear hysteretic dampers to meet an expected level of performance on structures under seismic excitation is proposed. The analysis is performed in the frequency domain including the nonlinear behavior of the dampers through the stochastic equivalent linearization of the Bouc–Wen [29] hysteretic model. Assuming that, in seismic problems, the main contribution to the total uncertainty is due to the excitation, a stationary stochastic process characterized by a power spectral density function compatible with the response spectrum defined by seismic code provisions was chosen to represent the excitation.

Through numerical examples, on different planar frames, the proposed procedure is demonstrated. In order to verify the efficiency of the optimization procedure and the validity of the results, nonlinear time history analysis using artificial ground motion records were performed.

2. Model of earthquake excitation

Studies on the efficiency of the dissipation systems and the influence of the excitation characteristics are usually carried out in time domain through Monte Carlo simulation using a sufficient number of deterministic artificially generated records [30]. However, in optimization problems with high computational cost due to numerous iterations, an alternative simple method is required. Spectral analysis, conducted in frequency domain, is an attractive method in which, a power spectral density function (PSDF), rather than a collection of time histories, can be advantageously used for modeling the excitation.

2.1. Derivation of design spectrum compatible power spectral density function

It is known that earthquake excitation is inherently random, however, if the evolution of the frequency content with time can be neglected, the input ground motion can be characterized by a power spectral density function (PSDF). In this study the earthquake excitation is assumed as a stationary Gaussian random process with zero mean represented by means of a design spectrum compatible PSDF. Following the methodology developed by Vanmarcke [31] cited in the work conducted by Giaralis and Spanos [32], the design spectrum compatible PSDF can be approximated by the following recursive equation:

$$G(\omega_j) = \frac{4\xi}{\omega_j\pi - 4\xi\omega_{j-1}}\left(\frac{S_a^2(\omega_j,\xi)}{\eta_j^2(\omega_j,\xi)} - \Delta\omega\sum_{k=1}^{j-1}G(\omega_k)\right) \quad \omega_j > \omega_0 \tag{1}$$

in which $G(\omega_j)$ and $S_a(\omega_j,\xi)$ are the one-sided PSDF and the median pseudo-acceleration response spectrum, respectively, at a specific frequency ω_j and $\xi = 0.05$ is the assumed damping ratio; $\Delta\omega$ is the frequency step in which the frequency range was discretized; the peak factor η_j is calculated by Eq. (2) and it represents the factor by which the rms value of the response of a SDOF oscillator must be multiplied to predict the level S_a below which the peak response of the oscillator will remain, with probability p, throughout the duration of the input process T_s. Herein, the following approximated semi-empirical formula for the calculation of the peak factor is adopted, which is known to be reasonably reliable for earthquake engineering applications [31]:

$$\eta_j = \sqrt{2\ln\left\{2\upsilon_j\left[1-\exp\left(-q_j^{1.2}\sqrt{\pi\ln(2\upsilon_j)}\right)\right]\right\}} \tag{2}$$

in which

$$\upsilon_j = \frac{T_s}{2\pi}\omega_j(-\ln p)^{-1} \tag{3}$$

and

$$q_j = \sqrt{1-\frac{1}{1-\xi^2}\left(1-\frac{2}{\pi}\tan^{-1}\frac{\xi}{\sqrt{1-\xi^2}}\right)} \tag{4}$$

Eqs. (3) and (4) are close form expressions derived for a white noise PSDF which has to be a priori assumed without knowledge of $G(\omega_j)$ when the peak factor is calculated by Eq. (2). $T_s = 20$ s is the duration assumed for the underlying stationary process; $p = 0.5$ is an appropriate probability assumed for the purposes of this study and $\omega_0 = 0.36$ rad/s denotes the lowest bound of the existence domain of Eq. (2) for a PSDF [32].

The power spectrum density estimation obtained by Eq. (1) can be improved via the following iterative scheme [32]:

$$G^{i+1}(\omega_j) = G^i(\omega_j)\left[\frac{S_a^t(\omega_j,\xi)}{S_a^i(\omega_j,\xi)}\right]^2 \tag{5}$$

in which $S_a^t(\omega_j,\xi)$ and $S_a^i(\omega_j,\xi)$ are the target design spectrum and the associated design spectrum estimated in the i-th iteration, respectively.

3. Evaluation of stochastic response

The equations of motion of an n-story planar frame structure provided with hysteretic perfectly elastoplastic dampers subjected to earthquake excitation may be written in the matrix form as [33]:

$$\mathbf{M}\ddot{\mathbf{x}}(t) + \mathbf{C}\dot{\mathbf{x}}(t) + \mathbf{K}\mathbf{x}(t) + \mathbf{K_h}\mathbf{X_y}\mathbf{z}(t) = -\mathbf{M}\mathbf{r}\ddot{x}_g(t) \tag{6}$$

where $\mathbf{M}$, $\mathbf{K}$ and $\mathbf{C}$ are the mass, stiffness and the proportional damping matrices of size $n \times n$, respectively; $\mathbf{K_h}$ is the pre-yielding stiffness matrix of the added hysteretic dampers of size $n \times n$, $\mathbf{X_y}$ is a diagonal matrix of the assumed yield displacement of each damper, $\mathbf{r}$ is the influence vector of size $n \times 1$, $\ddot{x}_g(t)$ is the horizontal acceleration of ground motion and $\ddot{\mathbf{x}}(t)$, $\dot{\mathbf{x}}(t)$ and $\mathbf{x}(t)$ are the generalized acceleration, velocity and displacement vectors of size $n \times 1$,

respectively. Assuming one device per story, $\mathbf{z}(t)$ is the vector of non-dimensional internal hysteretic variables satisfying the following nonlinear first order differential equation [29] for each device:

$$\dot{z}_i = x_y^{-1}\left(A\dot{u}_i - \gamma|\dot{u}_i|z_i|z_i|^{\eta-1} - \beta\dot{u}_i|z_i|^{\eta}\right) \quad i = 1,\ldots,n \tag{7}$$

where A, β, γ and η are non-dimensional parameters that characterize the hysteresis loop and are selected such that the predicted response from the model closely matches with the experimental results of the dampers [34]; $\dot{u}_i$ is the relative velocity between ends of dampers (usually, $\dot{u}_i = \dot{x}_i - \dot{x}_{i-1}$ being $\dot{x}_i$ the velocity of i-th story).

Since the analysis is performed in the frequency domain, the Eq. (7), representing the hysteretic force–deformation characteristics of the dampers, is linearized as [35,36]

$$\dot{z}_i = -k_{ei}z_i - c_{ei}\dot{u}_i \tag{8}$$

where k_{ei} and c_{ei} are the linearization coefficients, which are obtained by minimizing the mean square error between the linear and nonlinear terms of Eqs. (7) and (8). For $\eta = 1$, the equivalent constants k_{ei} and c_{ei} are given by:

$$k_{ei} = x_y^{-1}\sqrt{\frac{2}{\pi}}\left[\gamma\sqrt{E(\dot{u}_i,\dot{u}_i)} + \beta\frac{E(\dot{u}_i,z_i)}{\sqrt{E(z_i,z_i)}}\right] \tag{9}$$

$$c_{ei} = x_y^{-1}\left(\sqrt{\frac{2}{\pi}}\left[\beta\sqrt{E(z_i,z_i)} + \gamma\frac{E(\dot{u}_i,z_i)}{\sqrt{E(\dot{u}_i,\dot{u}_i)}}\right] - A\right) \tag{10}$$

where $E(.)$ is the expectation operator.

When the excitation is an uncorrelated shot noise (including white noise), Eqs. (6) and (8) can be written as the following system of first-order differential equations

$$\frac{d}{dt}\mathbf{y} = \mathbf{G}\mathbf{y} + \mathbf{w} \tag{11}$$

where $\mathbf{y}$ is the state vector

$$\mathbf{y} = \left\{\mathbf{x}^T \quad \dot{\mathbf{x}}^T \quad \mathbf{z}^T\right\}^T \tag{12}$$

$\mathbf{G}$ is the augmented system matrix

$$\mathbf{G} = \begin{bmatrix} [0] & [I] & [0] \\ -\mathbf{M}^{-1}\mathbf{K} & -\mathbf{M}^{-1}\mathbf{C} & -\mathbf{M}^{-1}\mathbf{K}_h\mathbf{X}_y \\ [0] & -\mathbf{C}_e\mathbf{T} & -\mathbf{K}_e \end{bmatrix} \tag{13}$$

in which [0] and [I] denotes the null and identity matrix, respectively, of size $n \times n$; $\mathbf{M}^{-1}$ is the inverse of mass matrix $\mathbf{M}$, $\mathbf{C}_e$ and $\mathbf{K}_e$ are diagonal matrices of the linearization coefficients (Eqs. (9) and (10)); $\mathbf{T}$ is a constant matrix consisting of 1, −1 and 0 and $\mathbf{w}$ is the excitation vector given by:

$$\mathbf{w} = \left\{\{0\} \quad \{0\} \quad -\{1\}\ddot{x}_0\right\}^T \tag{14}$$

where {0} and {1} denotes the null and unit vector, respectively, of size $1 \times n$; and $\ddot{x}_0(t)$ denotes the ground motion assumed as a zero-mean white noise random process with a constant PSDF of intensity, S_o.

Let the covariance matrix of $\mathbf{y}$ be $\mathbf{S}$ with

$$S_{ij} = E(y_i y_j) \tag{15}$$

in which $E(.)$ is the expectation operator and y_i is the i-th element of vector $\mathbf{y}$.

It can be shown [30] that for zero-mean white noise random process, the matrix $\mathbf{S}$ satisfies the following differential equation:

$$\frac{d}{dt}\mathbf{S} = \mathbf{G}\mathbf{S}^T + \mathbf{S}\mathbf{G}^T + \mathbf{D} \tag{16}$$

in which $\mathbf{D}$ is a matrix of the expected values of the product between excitation and state vectors being $D_{ij} = E(y_i\, z_j) = 0$ except that $D_{3n,3n} = 2\pi\, S_0$.

Since the excitation is assumed stationary, the matrix $\mathbf{D}$ is time independent, then, the stationary solution of Eq. (16) can be obtained by solving the following Lyapunov matrix equation

$$\mathbf{G}\mathbf{S}^T + \mathbf{S}\mathbf{G}^T + \mathbf{D} = \mathbf{0} \tag{17}$$

Note that the covariance matrix $\mathbf{S}$ is obtained by solving the Eq. (17) for a white noise type excitation with constant PSDF; however, Eq. (5) represents the PSDF of the stationary Gaussian random process, $\ddot{x}_g(t)$. This obstacle can be circumvented by filtering the white noise $\ddot{x}_0(t)$ through two linear filters as follows:

$$\ddot{x}_g(t) + 2\xi_g\omega_g\dot{x}_g(t) + \omega_g^2 x_g(t) = -\left(\ddot{x}_f(t) + \ddot{x}_0(t)\right), \tag{18}$$

$$\ddot{x}_f(t) + 2\xi_f\omega_f\dot{x}_f(t) + \omega_f^2 x_f(t) = -\ddot{x}_0(t) \tag{19}$$

in which ω_g, ξ_g, ω_f and ξ_f are the ground filter parameters. Eqs. (18) and (19) lead to the following Clough and Penzien stationary PSDF [37]

$$G_{CP}(\omega_j) = S_0\left(\frac{1 + 4\xi_g^2(\omega_j/\omega_g)^2}{\left[1 - (\omega_j/\omega_g)^2\right]^2 + 4\xi_g^2(\omega_j/\omega_g)^2}\right)\left(\frac{(\omega_j/\omega_f)^4}{\left[1 - (\omega_j/\omega_f)^2\right]^2 + 4\xi_f^2(\omega_j/\omega_f)^2}\right) \tag{20}$$

Thus, to make compatible the PSDF given by Eqs. (5) and (20), the filter parameters are estimated by fitting both functions.

On the basis of the above considerations, the stochastic structural response is obtained by solving the Eq. (17) in which, the state vector, $\mathbf{y}$, the augmented system matrix, $\mathbf{G}$, and excitation vector, $\mathbf{w}$, can be re-written as follows:

$$\mathbf{y} = \left\{\mathbf{x}^T \quad \dot{\mathbf{x}}^T \quad \mathbf{z}^T \quad x_f \quad \dot{x}_f \quad x_g \quad \dot{x}_g\right\}^T \tag{21}$$

$$\mathbf{G} = \begin{bmatrix} [0] & [I] & [0] & \{0\}^T & \{0\}^T & \{0\}^T & \{0\}^T \\ -\mathbf{M}^{-1}\mathbf{K} & -\mathbf{M}^{-1}\mathbf{C} & -\mathbf{M}^{-1}\mathbf{K}_h\mathbf{X}_y & -\{1\}^T\omega_f^2 & -\{1\}^T 2\xi_f\omega_f & \{1\}^T\omega_g^2 & \{1\}^T 2\xi_g\omega_g \\ [0] & -\mathbf{C}_e\mathbf{T} & -\mathbf{K}_e & \{0\}^T & \{0\}^T & \{0\}^T & \{0\}^T \\ \{0\} & \{0\} & \{0\} & 0 & 1 & 0 & 0 \\ \{0\} & \{0\} & \{0\} & -\omega_f^2 & -2\xi_f\omega_f & \omega_g^2 & 2\xi_g\omega_g \\ \{0\} & \{0\} & \{0\} & 0 & 0 & 0 & 1 \\ \{0\} & \{0\} & \{0\} & 0 & 0 & -\omega_g^2 & -2\xi_g\omega_g \end{bmatrix} \tag{22}$$

$$\mathbf{w} = \left\{\{0\} \quad \{0\} \quad \{0\} \quad 0 \quad 0 \quad 0 \quad -\ddot{x}_0\right\}^T \tag{23}$$

and the elements of the covariance matrix $\mathbf{D}$ of size $3n + 4 \times 3n + 4$ are $D_{ij} = 0$ except that $D_{3n+4,3n+4} = 2\pi\, S_0$.

It can be observed from Eqs. (9) and (10) that, the linearization coefficients depend on the response through $\mathbf{S}$, so an iterative procedure is required. The initial values of the coefficients can be arbitrarily chosen and the convergence is achieved after a few iterations [38].

4. Optimal placement of hysteretic dampers

4.1. Optimization problem

The challenge of the optimization problem to place hysteretic dampers consists in finding the capacities of the added dampers in each story, f_{yi}, expressed as a vector of yielding forces $\mathbf{f_y} = \{f_{yi}\}$, which minimize a given objective function. Then, the optimization problem is stated as follows:

$$\min_{\mathbf{f_y}} \quad f(\mathbf{f_y}) \tag{24}$$

subject to the constraints on the total added capacity and the yielding force of each damper given by:

$$\sum_{i=1}^{n} f_{y_i} = \overline{W}, \quad i = 1, \ldots, n \tag{25}$$

$$0 \leqslant f_{y_i} \leqslant \overline{W} \tag{26}$$

where $\overline{W}$ is the total dissipation capacity needed to achieve the required structural performance.

4.2. Objective function: sum of maximum interstory drift and base shear force

It is clear that to determine the locations and sizes of hysteretic dampers, the minimization of the interstory drifts is essential [7,8]. However, the structural deformation reduction can be achieved by increasing the stiffness, which can lead to an increase of the base shear force. Therefore, both, interstory drift and base shear force should be considered in the optimization problem. Accordingly, the objective function to be minimized may be stated as the sum of the root mean square values (rms) of maximum interstory drift and base shear force, both, relative to the values obtained on the uncontrolled structure (without added dampers). Thus, Eq. (24) takes the form:

$$\min_{\mathbf{f_y}} \left(\frac{\sigma_{d\max}}{\sigma_{d_0 \max}} + \frac{\sigma_v}{\sigma_{v_0}} \right), \tag{27}$$

where the subscript 0 indicates values of the original structure and

$$\sigma_{d\max} = \max\left(\sigma_{d_1}, \sigma_{d_2}, \ldots, \sigma_{d_n}\right), \tag{28}$$

in which the vector of the rms values of interstory drifts can be obtained as [39]

$$\boldsymbol{\sigma}_{\mathbf{d}} = diag\left(\mathbf{T}\mathbf{S}\mathbf{T}^T\right)^{1/2}, \tag{29}$$

where $\mathbf{T}$ is a constant matrix consisting of 1, −1 and 0 and the covariance matrix $\mathbf{S}$ is obtained by solving the Eq. (17). The rms value of base shear force can be obtained as follows [39]

$$\sigma_v = \left(\mathbf{r}^T\mathbf{V}\mathbf{S}\mathbf{V}^T\mathbf{r}\right)^{1/2} \tag{30}$$

in which the auxiliary matrix $\mathbf{V}$, of size $n \times 3n + 4$, is defined by:

$$\mathbf{V} = \lfloor \mathbf{K} \quad \mathbf{C} \quad \mathbf{K_h X_y} \quad \{0\}^T \quad \{0\}^T \quad \{0\}^T \quad \{0\}^T \rfloor \tag{31}$$

4.3. Required performance

Limitations on interstory drift are given by seismic design code provisions to control deformations and to prevent potential instabilities in both structural and non-structural elements. To define the minimum capacity of the dissipation system, the peak of the maximum interstory drift was adopted as performance criterion. In accordance with the provision of the IBC 2003 [40] and other outstanding seismic codes, for a typical shear structure similar to those used in the next examples, the limit of maximum interstory drift is 1.0%, which will be assumed as level of performance required for the dissipation system design.

For a given excitation, the mean peak of the maximum interstory drift can be calculated from the root mean square value determined by Eq. (28) as follows [41]:

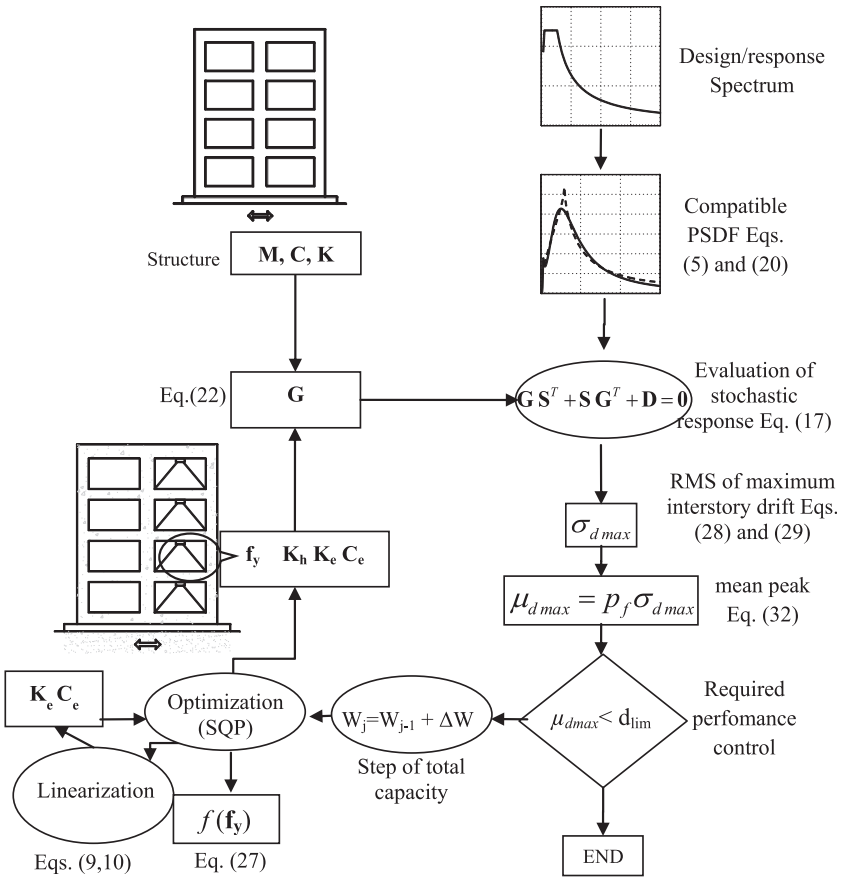

Fig. 1. Flowchart of the proposed methodology.

$$\mu_{d\max} = p_f \sigma_{d\max}, \tag{32}$$

$$p_f = \sqrt{2\ln \nu_e \tau} + \frac{0.5775}{\sqrt{2\ln \nu_e \tau}}, \tag{33}$$

where $\mu_{d\max}$ is the mean peak of the maximum interstory drift, p_f is the peak factor, $\sigma_{d\max}$ is the rms value of the maximum interstory drifts, ν_e is the modified mean zero-crossing rate, and τ is the time duration of the excitation. Kieureghian [41] derived a simple expression for ν_e from a SDOF subjected to white noise ground acceleration given by

$$\nu_e = \begin{cases} (1.90\xi^{0.15} - 0.73)\nu, & (\xi < 0.54) \\ \nu, & (\xi \geqslant 0.54) \end{cases} \tag{34}$$

where

$$\nu = \frac{\omega_1}{\pi} \tag{35}$$

in which ν is the zero-crossing rate of the response, and ω_1 and ξ are the natural frequency and the critical damping ratio of the SDOF structure, respectively. For multi-degree-of-freedom (MDOF) structures, both parameters of the fundamental vibration mode are used under the assumption that the fundamental mode dominates the dynamic response.

4.4. Optimization procedure

In this study, the optimization problem stated by Eqs. (24)–(26), is solved by using an iterative algorithm that includes a Sequential Quadratic Programming (SQP) method [42,43]. The algorithm finds sequentially the dissipation capacity, f_{yi}, in every possible location (in this study, one damper in each story is assumed) for a gradual increase in the total capacity until the required performance is achieved.

The flowchart of Fig. 1 summarizes the proposed methodology as follows: Having defined the excitation PSDF, the proposed procedure starts by estimating the stochastic response (Eq. (17)) considering the structure without added dampers. The mean peak of the maximum interstory drift calculated from Eqs. (28), (29), and (32) is compared with the limit provided by the seismic code provision. If the desired performance level is achieved, the procedure ends, else, the total dissipation capacity $\overline{W}$ is increased by an appropriate step ΔW. The vector of the capacities of added dampers $\mathbf{f_y}$ is optimally determined through the SQP algorithm, taking into account the selected objective function. In every step of the SQP algorithm, an iterative procedure is required to determine the linearization coefficients according to Eqs. (9) and (10). Once $\mathbf{f_y}$ has been optimally calculated, the pre-yielding stiffness matrix of the added dampers $\mathbf{K_h}$ is assembled [33] from the pre-yielding stiffness of each damper determined as:

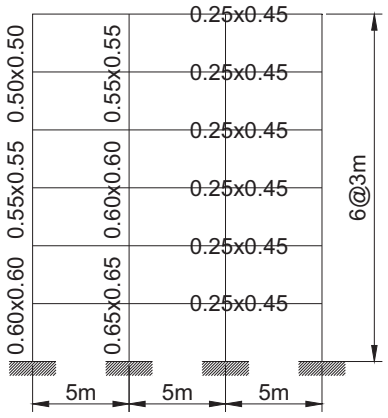

Fig. 2. Reinforcement concrete structure. (Example 1) [44].

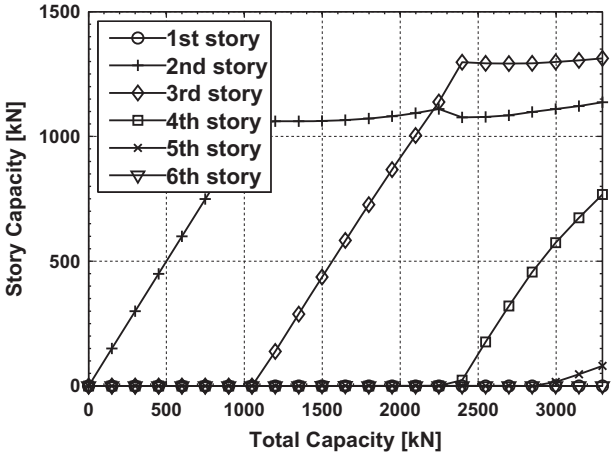

Fig. 4. Dissipation capacity distribution vs. total added capacity.

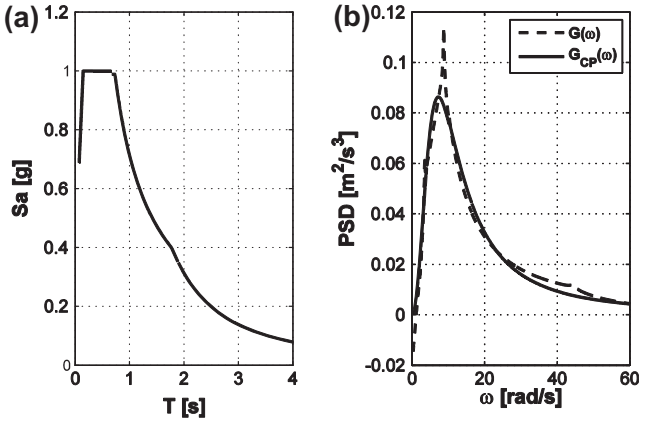

Fig. 3. Excitation characterized by: (a) IC 103 design spectrum and (b) design spectrum compatible PSDF.

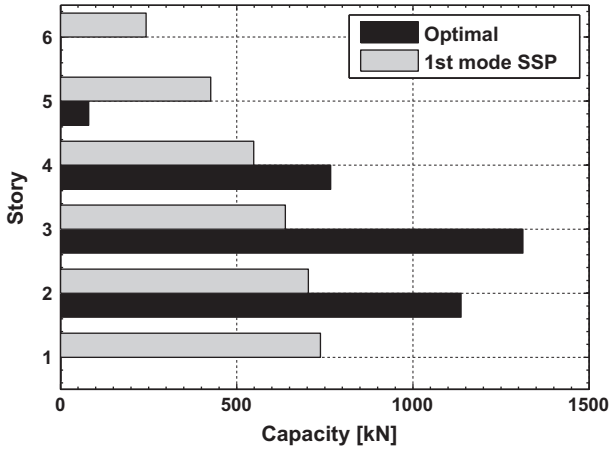

Fig. 5. Final damper distribution for the required performance (max drift = 1.0%).

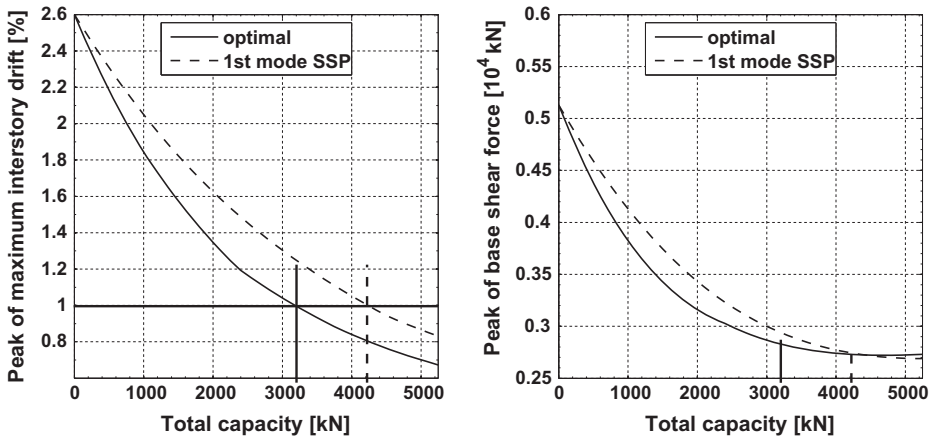

Fig. 6. (a) Peak of the maximum interstory drift; and (b) peak of base shear force.

$$k_{hi} = \frac{f_{yi}}{x_{yi}} \tag{36}$$

Thus, the augmented matrix **G** (Eq. (22)) is updated with the matrices, $\mathbf{K_h}$, $\mathbf{K_e}$ and $\mathbf{C_e}$ (Eqs. (9) and (10)) to re-evaluate the stochastic response (Eq. (17)). The procedure continues until the expected level of performance is achieved.

5. Numerical examples

5.1. Example 1: 6 story concrete building frame

The first example consists of a three bays, six-stories high reinforced concrete frame [44], in a building designed in accordance with the provisions of the Argentine Code IC103 [45]. Fig. 2 shows the geometric characteristics of the structure. The total mass per floor is 1×10^5 kg, Young's modulus of concrete $E = 24{,}800$ MPa which lead to a fundamental period $T_1 = 1$ s. The internal damping was adopted equal to 5% of critical damping ratio. It is important to note that a linear behavior was assumed to the structure and the nonlinearities were concentrate in the dissipation devices, which were represented by the elastoplastic Bouc–Wen model with shape parameters assumed constant equal to $x_y = 0.005$ m; $A = 1$; $\beta = \gamma = 0.5$; $\eta = 1$. Excitation was defined from pseudo-acceleration response spectrum for seismic zone 4 and soil profile type II given by IC 103 [45] which it is shown in Fig. 3(a). The corresponding compatible PSDF obtained by Eq. (5) (dashed line) and the Clough–Penzien approach (Eq. (20)) (continuous line) are displayed in Fig. 3(b).

Fig. 4 shows the optimal damper placement for increasing dissipation capacity obtained by using the proposed methodology. As can be observed, different damper locations are found for different total capacities, showing that the distribution of the dampers changes for different levels of desired performance.

The final distribution of added dampers that leads to the required level of performance (max interstory drift = 1.0%) is presented in Fig. 5. For comparison purposes, a 1st mode story shear proportional distribution [46] is also included. The required total dissipation capacity of 3297 kN is mainly distributed between the 2nd and 4th story, with capacities of 1137, 1313 and 767 kN respectively and, to a lesser extent, in the fifth story (80 kN).

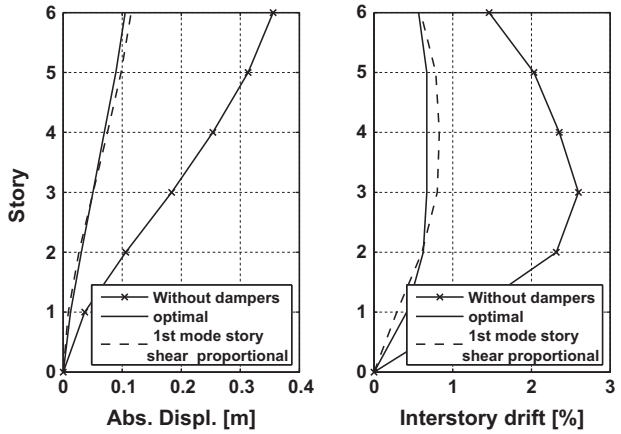

(a) peak absolute displacements. (b) peak interstory drift.

Fig. 7. Structural response for different designs (total installed capacity, 3297 kN).

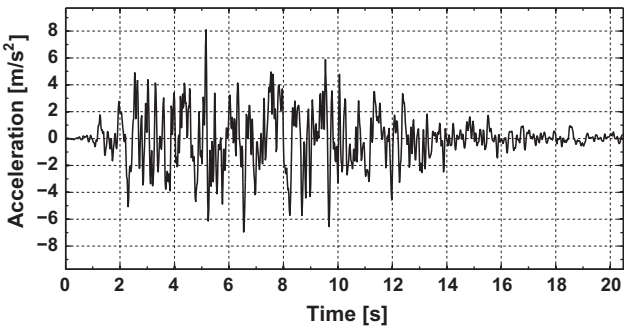

Fig. 8. Artificial ground motion record, compatible with IC 103 design spectrum.

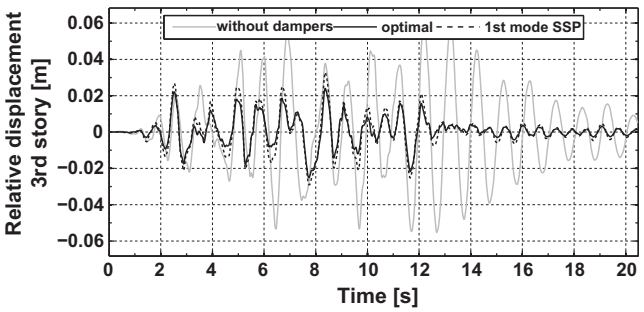

Fig. 9. Time history of the 3rd story relative displacement.

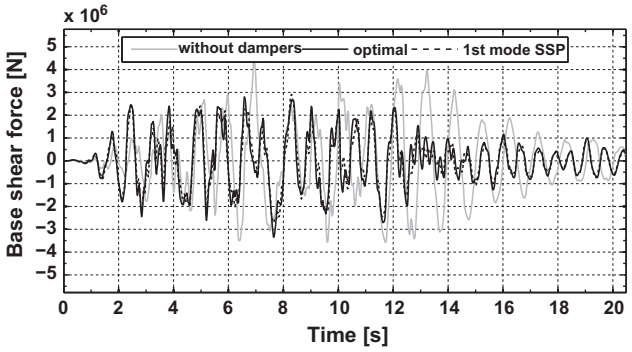

Fig. 10. Time history of the base shear force.

Table 1
Rms values of interstory drift obtained in the frequency domain and from nonlinear dynamic analysis for 100 artificial ground motions.

Story	Rms values of interstory drift (optimal design)		
	Frequency domain	Nonlinear dynamic analysis	Difference (%)
1	0.1937	0.2061	−6.0165
2	0.3216	0.3269	−1.6213
3	0.3653	0.3325	9.8647
4	0.3653	0.3378	8.1409
5	0.3564	0.3796	−6.1117
6	0.2777	0.3007	−7.6488

Fig. 6(a) and (b) shows the reduction of the peak of the maximum interstory drift and base shear force with increasing total capacity. Thus, it can be appreciated that the optimal placement obtained by the proposed procedure leads to a lower interstory drift and base shear force than the story shear proportional (SSP) distribution up to a total capacity of 4400 kN.

It can also be noted that, the proposed optimal solution requires about 32% less of installed capacity than the 1st mode story shear proportional distribution to achieve the desired level of performance (max interstory drift = 1.0%).

The structural responses for both damper distributions with a total capacity of 3297 kN are displayed in Fig. 7. It can be observed (Fig. 7(a)) that both designs lead to an important reduction of the absolute displacements respect to the structure without external dissipation. Clearly, Fig. 7(b) shows a significant efficiency of the proposed procedure, given that with the same installed capacity, the optimal damper distribution reduces the maximum interstory drift about 22% when compared to the story shear proportional distribution and 62% with respect to the uncontrolled structure.

5.2.1. Verification by time history analysis

To verify the validity of the proposed methodology, a nonlinear time history analysis was performed using a set of 100 artificial ground motion records [47], compatible with the IC 103 design spectrum. Fig. 8 shows one example of those records.

The relative displacement of the 3rd story for the aforementioned record is shown in Fig. 9. As expected, the peaks of relative displacement of the 3rd story obtained through optimal design remain below those obtained through a 1st mode story shear proportional distribution. It can also be observed that the maximum peak of the relative displacement obtained by the proposed procedure is 0.02956 m, which corresponds to an interstory drift of 0.985%, slightly below the expected level of performance (max drift = 1.0%).

While base shear force does not display major differences between both damper distributions (Fig. 10), it is clear the reduction with respect to uncontrolled structure.

To confirm the validity of the proposed procedure, the mean rms values of interstory drifts obtained via nonlinear dynamic analysis with the 100 artificial ground motions and those obtained in frequency domain through the proposed procedure are compared in Table 1. As can be observed, the differences are lower than 10%.

5.3. Example 2: 15 story steel building frame

This example consists of four steel moment-resisting frames in each direction, 15-stories high, in a building with two planes of symmetry [48]. Fig. 11 shows the geometric characteristics of the

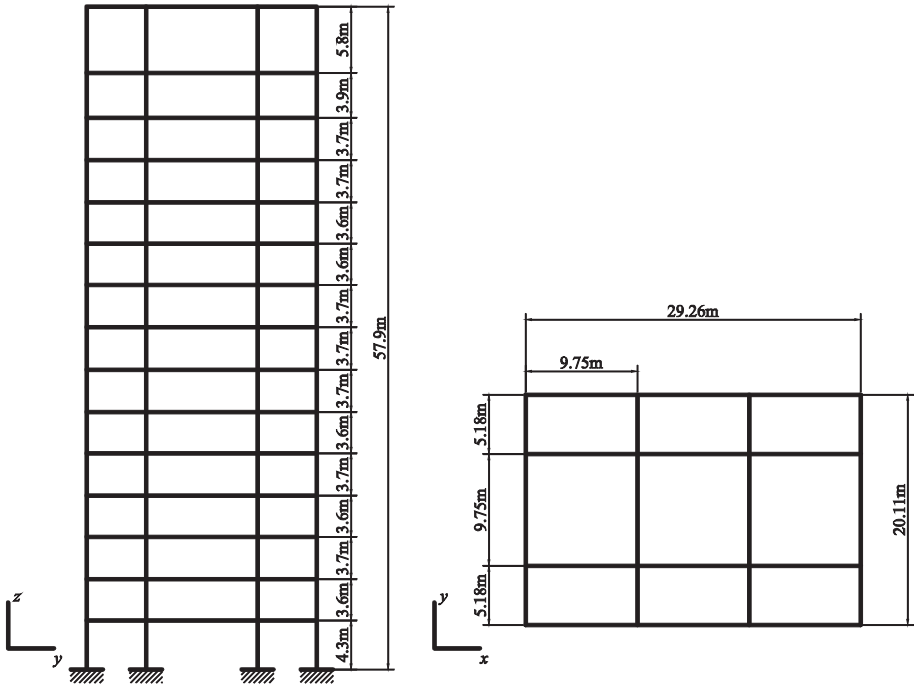

Fig. 11. Steel structure (Example 2) [48].

structure, the mass per floor and story stiffness on the z–y plane are indicated in Table 2. For low amplitude vibration, the fundamental period resulted equal to $T_1 = 1.89$ s. The internal damping was adopted equal to 2% of critical damping ratio. As in the preceding example the structural behavior was assumed linear and the nonlinearities of the dissipation devices were represented by the elastoplastic Bouc–Wen model with shape parameters assumed constant equal to $x_y = 0.01$ m; $A = 1$; $\beta = \gamma = 0.5$; $\eta = 1$.

Excitation was defined from the pseudo-acceleration response spectrum (Fig. 12(a)) for seismic zone 4, soil profile type SB, and seismic source type A, with a closest distance of 5 km to known seismic source given by UBC 97 [49]. The corresponding compatible PSDF obtained by Eq. (5) (dashed line) and the Clough–Penzien approach (Eq. (20)) (continuous line) are displayed in Fig. 12(b).

Fig. 13 shows the optimal damper placement for increasing dissipation capacity. The procedure indicates that, in order to efficiently meet the required level of performance (max drift = 1.0%), the total capacity of 30,318 kN should be non-uniformly distributed between 1st and 7th story as outlined in Fig. 14. For comparison, the SSP distribution is also included.

The structural responses obtained through both damper distributions with the same total capacity (30 MN) and those corresponding to the uncontrolled structure are displayed in Fig. 15. As in the previous example, in Fig. 15(a) can be observed that the peak values of the absolute displacements are effectively reduced through added dampers. Furthermore, the optimal design displays a greater reduction in the maximum interstory drift (about 22%) with respect to the SSP distribution (Fig. 15(b)).

Table 2
Example 2: model properties.

Story	Mass per floor (106 kg)	Stiffness (10^8 N/m)
1	0.2464	4.905
2	0.3986	4.905
3	0.3932	4.905
4	0.3932	4.4145
5	0.3905	4.4145
6	0.3905	4.4145
7	0.3905	4.1202
8	0.3905	4.1202
9	0.3905	3.924
10	0.3905	3.924
11	0.3905	3.924
12	0.3905	3.924
13	0.3905	3.7278
14	0.5844	3.5316
15	0.3624	2.7468

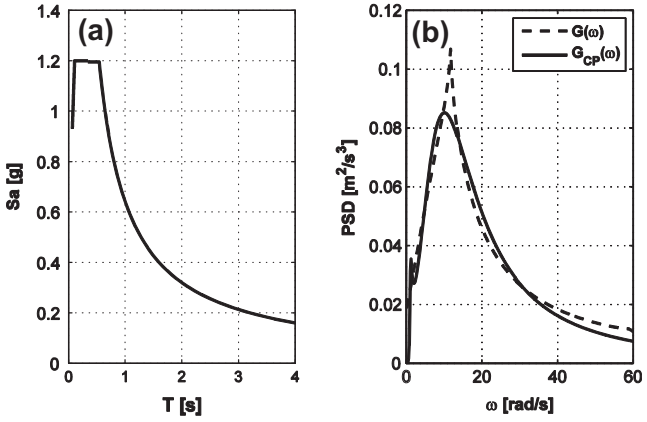

Fig. 12. Excitation characterized by: (a) UBC 97 design spectrum and (b) design spectrum compatible PSDF.

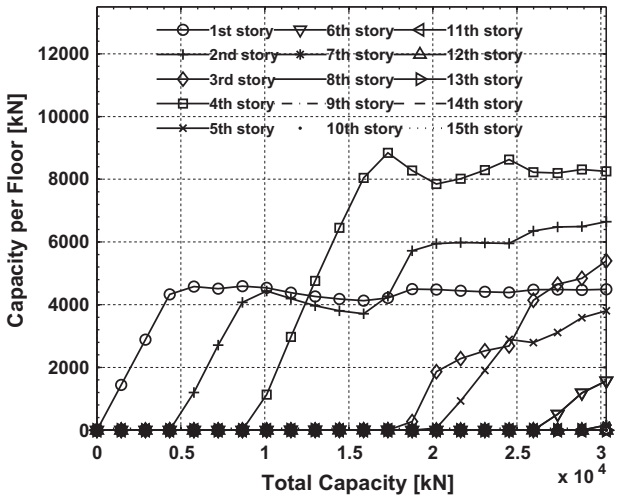

Fig. 13. Dissipation capacity distribution vs. total added capacity.

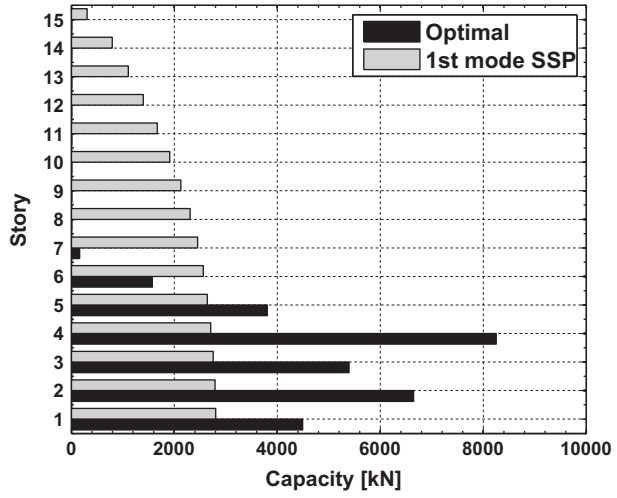

Fig. 14. Final damper distribution for the required performance (max drift = 1.0%).

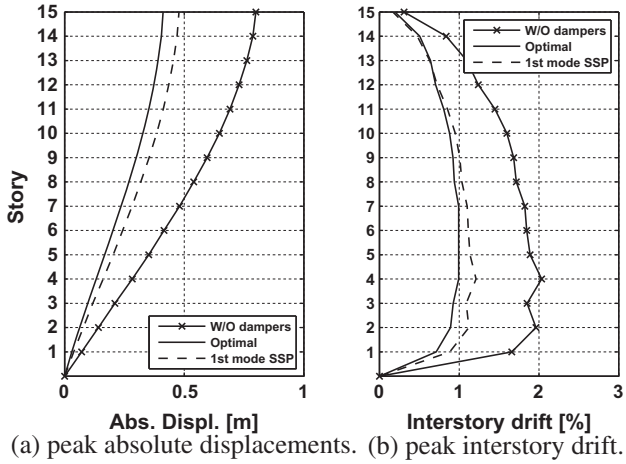

(a) peak absolute displacements. (b) peak interstory drift.

Fig. 15. Structural response for different designs (total installed capacity, 30 MN).

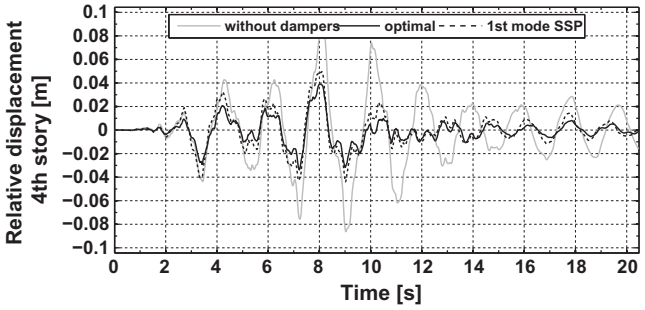

Fig. 16. Time history of the 4th story relative displacement.

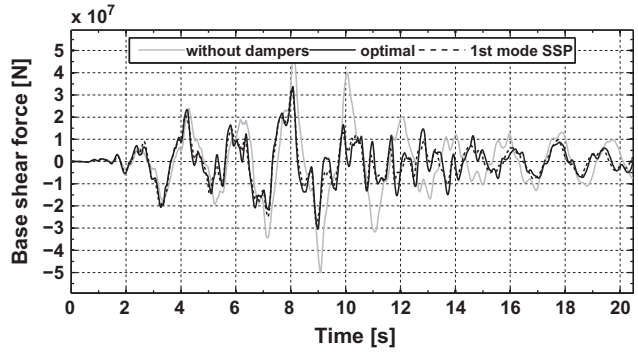

Fig. 17. Time history of the base shear force.

5.3.1. Verification by time history analysis

As before, a nonlinear time history analysis was performed using a set of 100 artificial ground motion records [47], compatible with the UBC 97 design spectrum.

The relative displacement for the first sample record of the 4th story (where drift is maximum) and base shear force are shown in Figs. 16 and 17, respectively. As expected, there is an important difference between both damper distributions in the relative displacement of 4th story and virtually negligible in the base shear force. It can also be observed that the maximum peak of the relative displacement obtained by the optimal distribution is 0.03906 m, which corresponds to an interstory drift close to target 1.0%.

As in the previous example, the differences between the mean rms values of interstory drift obtained via nonlinear dynamic analysis with 100 artificial ground motions and those obtained in frequency domain are lower than 10%.

6. Conclusions

Unlike others methods based on cumbersome procedures such as genetic algorithm and others, the paper presents a new and efficient methodology to optimally design passive nonlinear hysteretic energy dissipation systems in linear behaving buildings. The methodology allows defining the minimal energy dissipation capacity required to achieve a desired level of structural performance. According to the most important seismic codes provisions, the maximum allowed interstory drift was used as performance criterion. To ensure effective energy dissipation a linear combination between maximum interstory drift and base shear force is considered as objective function to be minimized. With the aim of achieving a robust design of the dissipation system, the structural response is stochastically determined in the frequency domain assuming as excitation a stationary stochastic process characterized by a design spectrum compatible power spectral density. This feature makes the procedure computationally efficient in contrast to other methods based on multiple time history analysis.

Through examples in planar frames, numerical results showed that with the optimal damper design, it can be achieved greater efficiency than with other damper distributions. The validity of the proposed procedure was confirmed by nonlinear dynamic analysis in time domain using artificial ground motion records.

Acknowledgement

The financial support of CONICET and National University of Cuyo is gratefully acknowledged.

References

[1] Takewaki I. Efficient redesign of damped structural systems for target transfer functions. Comput Methods Appl Mech Eng 1997;147:275–86.
[2] Takewaki I. Optimal damper placement for minimum transfer functions. Earthq Eng Struct Dyn 1997;26:1113–24.
[3] Takewaki I, Yoshitomi S. Effects of support stiffnesses on optimal damper placement for a planar building frame. Struct Des Tall Build 1998;7:323–36.
[4] Takewaki I. Optimal damper positioning in beams for minimum dynamic compliance. Comput Methods Appl Mech Eng 1998;156:363–73.
[5] Takewaki I, Yoshitomi S, Uetani K, Tsuji M. Non-monotonic optimal damper placement via steepest direction search. Earthq Eng Struct Dyn 1999;28:655–70.
[6] Takewaki I. Displacement–acceleration control via stiffness–damping collaboration. Earthq Eng Struct Dyn 1999;28:1567–85.
[7] Takewaki I. Optimal damper placement for critical excitation. Probab Eng Mech 1999;15:317–25.
[8] Takewaki I. Optimum damper placement for planar building frames using transfer functions. Struct Multidiscip Opti 2000;20:280–7.
[9] Takewaki I. An approach to stiffness–damping simultaneous optimization. Comput Methods Appl Mech Eng 2000;189:641–50.
[10] Cimellaro GP. Simultaneous stiffness–damping optimization of structures with respect to acceleration displacement and base shear. Eng Struct 2007;29:2853–70.
[11] Aydin E, Boduroglu MH, Guney D. Optimal damper distribution for seismic rehabilitation of planar building structures. Eng Struct 2007;29:176–85.
[12] Fujita K, Moustafa A, Takewaki I. Optimal placement of visco-elastic dampers and supporting members under variable critical excitations. Earthq Struct 2010;1:43–67.
[13] Singh MP, Moreschi LM. Optimal placement of dampers for passive response control. Earthq Eng Struct Dyn 2002;31:955–76.
[14] Bishop JA, Striz AG. On using genetic algorithms for optimum damper placement in space trusses. Struct Multidis Opt 2004;28:136–45.
[15] Singh MP, Moreschi LM. Optimal seismic response control with dampers. Earthq Eng Struct Dyn 2001;30:553–72.
[16] Uetani K, Tsuji M, Takewaki I. Application of an optimum design method to practical building frames with viscous dampers and hysteretic dampers. Eng Struct 2003;25:579–92.
[17] Ni YQ, Ko JM, Ying ZG. Random seismic response analysis of adjacent buildings coupled with non-linear hysteretic dampers. J Sound Vib 2001;246:403–17.
[18] Basili M, De Angelis M. Optimal passive control of adjacent structures interconnected with nonlinear hysteretic devices. J Sound Vib 2007;301(1–2):106–25.
[19] Ok SY, Song J, Park KS. Optimal design of hysteretic dampers connecting adjacent structures using multi-objective genetic algorithm and stochastic linearization method. Eng Struct 2008;30(5):1240–9.
[20] Moreschi LM, Singh MP. Design of yielding metallic and friction dampers for optimal seismic performance. Earthq Eng Struct Dyn 2003;32:1291–311.
[21] Jensen HA. Structural optimization of non-linear systems under stochastic excitation. Probab Eng Mech 2006;21:397–409.
[22] Vargas R, Bruneau M. Effect of supplemental viscous damping on the seismic response of structural systems with metallic dampers. J Struct Eng-ASCE 2007;133:1434–44.
[23] Vargas R, Bruneau M. Experimental validation of the structural fuse concept. In: 14th World conference on earthquake engineering. Beijing, China; 2008.
[24] Jensen HA, Valdebenito MA, Schuëller GI, Kusanovic DS. Reliability-based optimization of stochastic systems using line search. Comput Methods Appl Mech Eng 2009;198:3915–24.
[25] Jensen HA, Sepulveda JG. On the reliability-based design of structures including passive energy dissipation systems. Struct Safety 2012;34(1):390–400.
[26] Benavent-Climent A. An energy-based method for seismic retrofit of existing frames using hysteretic dampers. Soil Dyn Earthq Eng 2011;31(10):1385–96.
[27] Leu LJ, Chang JT. Optimal allocation of non-linear viscous dampers for three-dimensional building structures. Proc Eng 2011;14:2489–97.

[28] Ohsaki M, Nakajima T. Optimization of link member of eccentrically braced frames for maximum energy dissipation. J Constr Steel Res 2012;75:38–44.
[29] Wen YK. Method for random vibration of hysteretic systems. J Eng Mech Div ASCE 1976;EM2:249–63.
[30] Soong TT, Grigoriu M. Random vibration of mechanical and structural systems. New Jersey: Prentice Hall; 1993.
[31] Vanmarcke EH. Structural response to earthquakes. In: Lomnitz C, Rosenblueth E, editors. Seismic risk and engineering decisions. Amsterdam: Elsevier; 1976.
[32] Giaralis A, Spanos PD. Effective linear damping and stiffness coefficients of non-linear systems for design spectrum based analysis. Soil Dyn Earthq Eng 2010;30:798–810.
[33] Foliente GC. Stochastic dynamic response of wood structural systems. PhD. Diss., Virginia Polytechnic Institute and State University, Blacksburg, Virginia; 1993.
[34] Ikhouane F, Rodellar J. Systems with hysteresis. Analysis, identification and control using the Bouc–Wen model. Chichester (England): John Wiley & Sons Ltd.; 2007.
[35] Wen YK. Equivalent linearization for hysteretic systems under random excitation. J Appl Mech-ASME 1980;47:150–64.
[36] Roberts JB, Spanos PD. Random vibration and statistical linearization. Chichester, (UK): John Wiley & Sons; 1990.
[37] Clough RW, Penzien J. Dynamics of structures. 2nd ed. New York: McGrawHill; 1993.
[38] Sadek F, Ftima MB, El-Borgi S, McCormick J, Riley MA. Control of hysteretic structures using H_∞ algorithm and stochastic linearization techniques. In: Proc. seventh U.S. national conference earthquake eng. 2002; Boston, Massachusetts.
[39] De la Fuente E. An efficient procedure to obtain exact solutions in random vibration analysis of linear structures. Eng Struct 2008;30:2981–90.
[40] I.B.C. International Building Code. vol. 1–3; 2003.
[41] Der Kiureghian A. Structural response to stationary excitation. J Eng Mech Div ASCE 1980;106:1195–213.
[42] Arora JS. Introduction to optimum design. 2nd ed. San Diego: Elsevier Ltd.; 2004.
[43] Belegundu AD, Chandrupatla TR. Optimization concepts and applications in engineering. 2nd ed. New York: Cambridge University Press; 2011.
[44] Curadelli RO, Riera JD. Reliability based assessment of the effectiveness of metallic dampers in buildings under seismic excitations. Eng Struct 2004; 26:1931–8.
[45] INPRES-CIRSOC 103. Normas Argentinas para Construcciones Sismoresistentes; 1991.
[46] Hwang JS, Lin WC, Wu NJ. Comparison of distribution methods for viscous damping coefficients to buildings. Struct Infrastruct Eng 2013;9(1):28–41.
[47] Shinozuka M, Deodatis G. Simulation of stochastic processes by spectral representation. Appl Mech Rev 1991;44(4):191–205.
[48] Paz M. International handbook of earthquake engineering. Codes, programs, and examples. New York: Chapman & Hall; 1994.
[49] U.B.C. Uniform Building Code. vol. 1–3; 1997.